Appl. Phys. B 77, 497–503 (2003)
DOI: 10.1007/s00340-003-1264-x

Applied Physics B
Lasers and Optics

G. MICHAELI✉
A. ARIE

Optimization of quasi-phase-matched non-linear frequency conversion for diffusion bonding applications

Department of Electrical Engineering – Physical Electronics, Faculty of Engineering, Tel Aviv University, Tel-Aviv 69978, Israel

Received: 26 April 2003/Revised version: 25 June 2003
Published online: 23 September 2003 •

ABSTRACT The diffusion bonding technique has many applications in non-linear frequency-conversion processes. Unfortunately, when used for bonding periodically poled crystals, the periodic patterns have to be very precisely matched for efficient conversion. We investigated theoretically and experimentally this effect, in two configurations of increasing the length or the thickness of a crystal. We found that the sensitivity to the relative periodic domain match is much more severe for the case of increasing the crystal length with respect to increasing its thickness. Furthermore, even for symmetric pump illumination with respect to the interface between two crystals, an asymmetric intensity distribution may be obtained in the second harmonic. We have experimentally measured the second harmonic power modulation caused by varying the relative domain match at the interface between two attached, but unbonded crystals. A novel configuration for the domain patterns is proposed, which limits the degradation of the generated light caused by the domain mismatch.

PACS 42.65.Ky; 42.70.Mp; 77.84.-s

1 Introduction

Quasi-phase matching (QPM) in ferroelectric crystals is a well-established technique for efficiently generating coherent radiation at wavelengths for which direct and efficient lasing is difficult [1].

The QPM technique has several advantages that made it widely used lately, among which are the ability to engineer new processes using the highest non-linear coefficient of the crystal, the lack of double refraction, the ability to set the phase matching at a chosen temperature and wavelength, etc.

In using non-linear crystals for high-power applications, the damage threshold as well as thermal-lensing limitations require the use of thick and long crystals. Periodic poling technology and crystal-growth abilities have some limitations to produce thick and long periodically poled crystals. The thickness of the periodically poled crystals is limited in mature periodic poling techniques such as electric poling by technical complexities typically to 0.5–1 mm [2]. 3-mm-thick $RbTiOAsO_4$ (RTA) crystals have been periodically poled [3], but this cannot be achieved in many kinds of crystals, such as $KTiOPO_4$ (KTP) and $LiNbO_3$. Although there is a potential for direct poling of stoichiometric periodically poled $LiNbO_3$ (PPLN) and periodically poled $LiTaO_3$ (PPLT) using modest coercive fields (and hence a potential for thicker crystals), this potential has not been established yet. As the width of these crystals can be 30 times their thickness – elliptical beams can use the available aperture more effectively [4], however the need to shape the beam might cause difficulties and the method is not robust enough. The length of the crystal is also limited, by crystal-growth techniques, to lengths of ~ 50 mm in $LiNbO_3$ [5] and ~ 30 mm in KTP [6]. Several ways to overcome the length limitation have been offered including a double-pass configuration with wedged-crystal [7] or air-based [8, 9] phase correction. These methods are usually more complex than single-pass frequency conversion.

All these drawbacks can be overcome using the diffusion bonding (DB) technique, which enables a perfect optical connection between two originally separated crystals, as described by several authors for $LiNbO_3$ to $LiTaO_3$ bulk crystals [10], $LiNbO_3$ to $LiNbO_3$ bulk crystals [11], and periodically poled $LiNbO_3$ [12, 13]. The technique also embodies the potential for three-dimensional shaping of the non-linear coefficient. Diffusion bonding is also used to compensate walk-off in bulk KTP birefringently phase-matched frequency converters [14].

A drawback of this technique when used with periodically poled crystals is its high sensitivity to the relative period of the bonded crystals. This was first discussed by Missey et al. [12], for the case of increasing the cross section of the non-linear interaction by diffusion bonding two crystals. In the ideal case of a perfect match between the domains in the bonded crystals, the two bonded crystals will function as one thicker crystal. However, the domain matching is not perfect in general, causing a severe degradation in the non-linear process efficiency. Although domain self-adjustment had once been mentioned [13], the phenomenon has not been well established yet, and therefore we disregard it throughout this paper.

In this paper, the effect of efficiency degradation owing to domain mismatch between two bonded crystals is modeled for a second harmonic generation (SHG) process of Gaussian beams, using numerical simulation. Two different dif-

✉ Fax: +972-3/642-3508, E-mail: ady@eng.tau.ac.il

fusion bonding configurations were simulated for the cases of increasing the length and the thickness of a periodically poled material. The experimental and analytical results are presented for two periodically poled KTP (PPKTP) crystals, which are shifted one against the other in order to simulate different mismatches of domains.

In Sect. 2, the motivation for diffusion bonding periodically poled crystals will be reviewed, while in Sect. 3 the theoretical analysis and simulation algorithms for two configurations of increasing the length and the thickness of the crystal will be outlined. In Sect. 4 these simulation results are summarized. Section 5 deals with the experimental setup, whereas the experimental results in comparison to simulated results are described in Sect. 6. The main findings are finally discussed and summarized in Sect. 7.

2 Motivation for increasing length and thickness of periodically poled crystals

The motivation for increasing both the length and thickness of periodically poled crystals arises from aspects of thermal damage and thermal lensing. In general, the fundamental beam diameter might exceed the thickness of periodically poled materials. The thickness of the available crystals depends on the coercive field of the non-linear material, and on the required poling period. For PPKTP, the coercive field is about 120 kV/cm [15], and for frequency down-conversion processes into the mid-infrared range or for doubling long-wavelength sources, the typical periods are in the range of 20–40 μm. This limits the thickness of PPKTP crystals for the mentioned process to about 1–1.5 mm. For frequency up-conversion into the visible and ultraviolet range, the periods should be shorter than 10 μm and the crystal thickness is limited to thinner values of ∼ 0.5 mm. Further thickening of the input crystal can be achieved using the diffusion bonding of two non-linear crystals, which were periodically poled separately.

Let us consider a crystal with length L and thickness t, and a Gaussian beam having a beam waist ω_0 located in the middle of the crystal. Let us consider first the case of confocal focusing (see Fig. 1a), which is close to the optimal focusing. For this case, the confocal parameter $b = \omega_0^2 k_\omega$ is equal to L; hence $\omega_0 = \sqrt{L/k_\omega}$, where k_ω is the wave vector of the fundamental wave. In order to prevent beam clipping, the radius of the fundamental wave on the crystal output facet is set to one-third of the thickness. For the confocal case the beam waist has to fulfill the condition

$$\omega_0 \leq \frac{\text{thickness}}{3\sqrt{2}}\,; \tag{1}$$

hence for 0.5-mm and 1-mm-thick crystals the beam-waist radius must be smaller than 110 μm and 220 μm, respectively. However, the confocal lengths in these cases are usually much longer than practical crystal lengths, e.g. assuming 1064-nm pump in PPLN, the confocal lengths are 15.7 and 62.9 cm, respectively. This means that, from a geometrical perspective, there is no need to increase the thickness of crystals, but it may be worthwhile in some cases to increase their length, by diffusion bonding.

Since the crystal length is usually much smaller than the confocal parameter with loosely focused beams, we can neglect the beam divergence and assume that the beam radius at the crystal output facet is nearly identical to the beam waist (Fig. 1b). The criterion to avoid beam clipping in this case is simply

$$\omega_0 \leq \frac{\text{thickness}}{3}\,, \tag{2}$$

which for 0.5-mm and 1-mm-thick crystals corresponds to beam-waist radii of 166 μm and 333 μm, respectively.

In high-power applications, optical damage and thermal lensing might limit the process efficiency. Equation (2) can be used to determine the limits imposed by these two effects. For KTP the damage threshold is $D_{\text{th}} = 450\,\text{MW/cm}^2$ at $\lambda = 1.064$ μm for a pulse width of 10 ns and a repetition rate of 10 Hz. Assuming a 333-μm (166-μm) beam waist as derived above for a 1-mm (0.5-mm)-thick crystal, the laser pulse energy cannot exceed ≈ 16 mJ (4 mJ).

Thermal lensing, caused by the laser absorption and the temperature dependence of the refractive index in the crystal, is an even more compelling effect, in particular for cw applications. For a given pump power P, the minimal beam waist (and therefore crystal thickness, as $\omega_0 \sim$ thickness/3) allowed can be found by limiting the thermal lens focal length to a given value through the following ratio [16, 17]:

$$f_{\text{TL}} = \frac{\pi K_{\text{c}}}{\alpha\left(\dfrac{\text{d}n}{\text{d}T}\right) P \int\limits_{\substack{\text{crystal}\\ \text{length}}} \dfrac{\text{d}z}{\omega^2(z)}}\,, \tag{3}$$

where f_{TL} is the thermal lens focal length, K_c is the thermal conductivity, α is the power absorption coefficient, $\text{d}n/\text{d}T$ is the refractive-index dependence on temperature, and ω is the fundamental field radius. Let us assume that the thermal lensing can be neglected in a frequency-conversion process, provided that the thermal lens is larger than $f_{\text{min}} = 100$ mm. Hence, the maximal pump power allowed for a 1.064-μm pump in a 1-cm-long, 0.5-mm-thick crystal will be ∼ 4.75 W

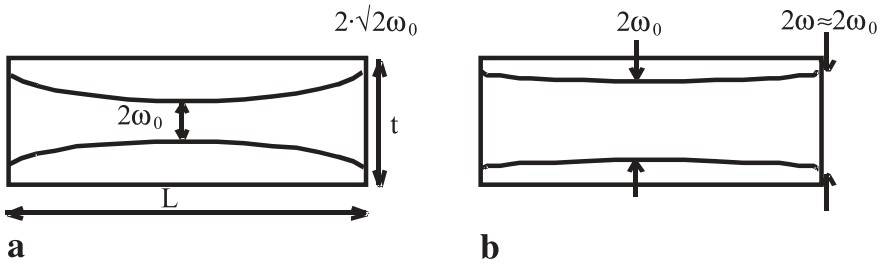

FIGURE 1 Crystal and fundamental-beam definitions: **a** confocal focusing, **b** loose focusing

for $LiNbO_3$ and ~ 21.2 W for KTP. The higher the power, the stronger the focusing will be, so at higher-power applications the use of a wide-diameter beam is a necessity.

These motivations, and the advantages of the diffusion bonding technique for overcoming the difficulties mentioned above, led us to consider the sensitivity of the technique to the phase mismatch between adjacent domains.

3 Theoretical analysis

For evaluating the effect of domain mismatch between diffusion bonded crystals, two configurations were considered: lengthening the crystal and thickening it. In both cases the effect of domain mismatch was analyzed for SHG.

Consider a non-linear crystal of length L, in which a fundamental Gaussian beam is propagating in the X crystallographic direction and focused at the center of the crystal (where the optimal focus is [18]). Since the relevant non-linear crystals have negligible absorption ($< 1\%$/cm) in the visible and near infrared, we have neglected the effect of absorption. Furthermore, as QPM is typically a type-I process, with all interacting waves polarized in the same direction, we assume that there is no walk-off. We also neglect pump depletion.

While propagating along the crystal, each crystal increment Δx contributes to the total generated field at the second harmonic, a contribution that can be described by a differential equation, following the terminology of [19] in CGS units:

$$\frac{\mathrm{d}E_{2\omega}}{\mathrm{d}x} = \frac{2\pi \mathrm{i}\omega_2}{cn_2} d_{ij}(x)\, E_\omega^2 \mathrm{e}^{\mathrm{i}\Delta k \cdot x}\,, \tag{4}$$

where $E_{2\omega}$ is the second-harmonic field, ω_2 and $n_{2\omega}$ are the angular frequency and the index of refraction of the crystal at the second harmonic respectively, c is the light velocity in vacuum, and $d_{ij}(x)$ is the x-dependent non-linear coefficient, equal to d_{33} or $-d_{33}$, depending on the direction of the non-linear susceptibility in the local domain. The contribution of each crystal increment can be propagated to the output facet of the crystal using the Fresnel-integral or the beam-propagation method (BPM). Summing the contributions of all increments yields the field distribution at the crystal output.

The optimization is performed over a set of focusing parameters ξ, for each of which inner optimization is carried over a set of wave-vector-mismatch parameters σ, where ξ is defined by $\xi = L/b$ and σ is defined by:

$$\sigma = \frac{b\Delta k}{2}\,, \tag{5}$$

where $\Delta k = 2k_\omega - k_{2\omega}$ is the wave-vector mismatch.

An analytical equation that enables us to calculate the second-harmonic power for the case of perfect domain matching in a loss-less crystal is given by [19]:

$$P_{2\omega} = \frac{128\pi^2\omega_1^2 d_{\mathrm{eff}}^2 P_\omega^2 L k_\omega h(\sigma, \xi)}{c^3 n_\omega^2 n_{2\omega}}\,, \tag{6}$$

where ω_1 is the angular frequency of the fundamental beam, P_ω is the power of the fundamental beam, n_ω is the refractive index of the fundamental, h is the Boyd–Kleinmann focusing parameter [19], and d_{eff} is the effective non-linear coefficient, equals to $(2/\pi d_{33})$. The simulations described in the following paragraphs were compared to (6) for the degenerate case of perfect domain matching.

In order to numerically evaluate the expected dependence of SHG efficiency on the relative domain mismatch in increasing the length or the thickness of the crystal, a beam-propagation simulation, based on the Fresnel diffraction integral, was written. The simulation is general in the way that it uses an arbitrary field distribution as an input, and can be easily extended to other frequency-mixing processes, as well as to different cases of modulating the non-linear coefficient, e.g. two-dimensional modulation of the non-linear coefficient [20].

The Fresnel diffraction integral [21] is a useful tool for propagating an arbitrary field distribution through a medium. First, the fundamental or second-harmonic field is decomposed using the discrete Fourier transform into two-dimensional spatial frequency components that represent a series of plane waves. Each of these plane waves propagates at a different spatial angle, and its wave-vector transverse components are given by k_y, k_z, corresponding to the spatial frequencies ν_y, ν_z, defined by $\nu_y = 2\pi/k_y$ and $\nu_z = 2\pi/k_z$. This decomposition enables us to propagate the field to the output facet of the non-linear crystal, using the simple transfer function:

$$H\left(\nu_y, \nu_z\right) = \mathrm{e}^{\mathrm{i}kD}\, \mathrm{e}^{-\mathrm{i}\pi\lambda D\left(\nu_y^2+\nu_z^2\right)}\,, \tag{7}$$

where D is the distance of field propagation. At the output facet, the field distribution is summed for all Δx increments, and then reconstructed using the inverse Fourier transform to form the final output distribution.

In some selected cases, the simulation results were compared to an independent calculation based on the beam-propagation method [22, 23]. Both simulation methods yielded the same results.

The lateral dimensions of the crystal are assumed to be large enough, in comparison to the beam dimensions, so that beam-clipping effects are negligible. The fundamental field and second harmonic field distributions are expressed using matrix representation. Simulation run time is strongly dependent on both transverse and longitudinal sampling resolutions. Therefore the matrix size is chosen to have the minimal size that keeps the SHG power dependence on the size within the required accuracy, at a given lateral sampling resolution. Hence, a trade-off between the waist and the beam diameter at the output facet takes place. The simulation used the same matrix size (of 128×128) but different lateral sampling resolution for the wide range of focusing parameters ($0.1 \leq \xi \leq 10$). The lateral sampling resolution used was 0.25–0.5 μm for this range of focusing parameters (from symmetry considerations both vertical and horizontal resolutions are the same). The domain walls of the periodically poled crystal are perpendicular to the direction of propagation. The propagation is divided into small propagation increments Δx. These increments are chosen to be sufficiently short so that the generated power is independent of the increment size. Although the maximal period can theoretically be the length of the coherence length $L_c = \lambda_\omega/4(n_{2\omega} - n_\omega)$, smaller increments of $L_c/16$ were taken to provide the required accuracy.

4 Simulation results

The beam propagation simulation program, based on the Fresnel integral, was written to simulate two cases of increasing the length or the thickness of the non-linear crystal. The simulation was compared to the analytical equation given in (6), for the degenerate case of perfect domain matching, yielding an excellent agreement for perfect Gaussian beams.

4.1 *Increasing the crystal length*

This simulation accurately describes the experimental setup of Fig. 6. Several cases of mismatch between the relative domains of the crystals were assumed, from $\Delta L = 0$ to $\Delta L = L_c$. The simulation first finds the optimized wave-vector mismatch $\sigma(\Delta L = 0)$ for several focusing parameters $0.1 < \xi < 4$. For each of those ξ (and their corresponding optimal σ), it numerically finds the second-harmonic power generated (marked by + signs in Fig. 2), which are in excellent agreement with the analytical results (marked by the solid line), with an accuracy better than 2.2%. Then it numerically calculates the SHG power for different $\Delta L = L_c/4$, $L_c/2$, $3L_c/4$, L_c. For a given focusing parameter ξ, the power is modulated continuously while moving the crystal as a result of passing from perfect phase matching to phase mismatching – where the second-harmonic field generated in the first crystal is in opposite phase to the field generated in the second crystal. The period of full modulation is exactly the period of the domain reverse in the crystal, $2L_c$. The simulation assumes no losses inside the crystals and no Fresnel reflections between them.

From Fig. 2 one can see that the domain mismatch can lead to complete destruction of the second-harmonic wave. This happens for every focusing parameter ξ, resulting from a destructive interference of the fields generated in the two different crystals.

4.2 *Increasing the crystal thickness*

A similar calculation simulated two crystals attached one on top of the other. In this simulation two identical periodically poled crystals were assumed, where the relative phase of the domains is obtained by changing the sign of the non-linear coefficient inside one of the crystals without moving it physically from its original position. The simulation finds the optimized wave-vector mismatch σ for several focusing conditions ($0.1 < \xi < 20$). For each ξ and its corresponding optimal σ, the second-harmonic power is calculated for several relative mismatches between the domains of the two crystals (see Fig. 3). The case of no phase mismatch between the two crystals ($\Delta L = 0$), marked by + signs in Fig. 2, was found to be in good agreement with the analytic result, using (6), marked by the solid line, with an accuracy better than 4.8%. The simulation assumes no losses inside the crystals and no Fresnel reflections between them.

From Fig. 3, one can see that the power penalty owing to domain mismatch is negligible at weak focusing ($\xi = 0.1$), but may reach 66% at tight focusing ($\xi = 5$). Hence, for a weakly focused beam, the tolerance to domain phase error is larger.

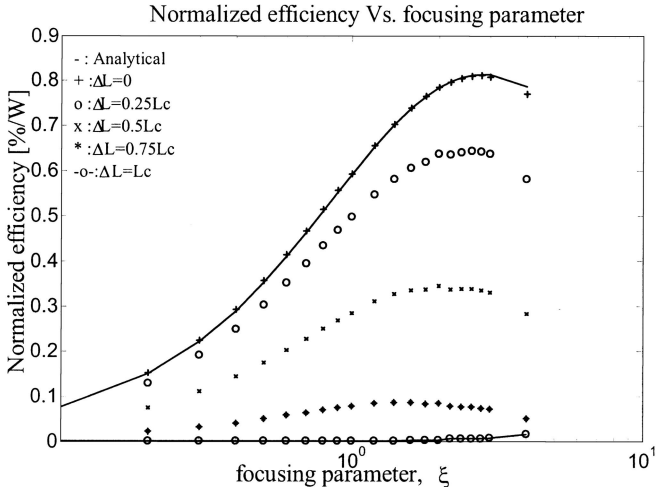

FIGURE 2 Normalized efficiency of SHG power generated in 27-mm-long PPKTP crystal pair (each with length of 14 mm with intersection of 1-mm length). 1-W input power at 1.55 μm was used, for several cases of mismatch between the domains of the two attached crystals. The analytical value is calculated based on (6), and marked by a *solid line*. The numerical results are marked by + for $\Delta L = 0$, by o for $\Delta L = 0.25L_c$, by x for $\Delta L = 0.5L_c$, by $*$ for $\Delta L = 0.75L_c$, and by –o– for $\Delta L = L_c$

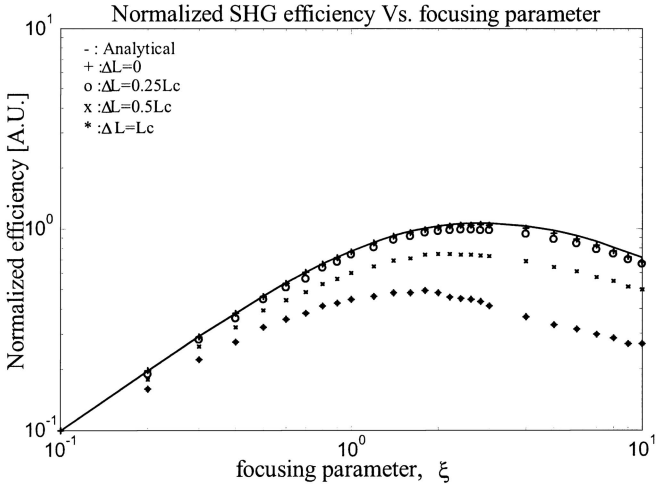

FIGURE 3 Normalized efficiency of SHG power generated in 1-cm-long PPKTP crystal pair. 1-W input power at 1.55 μm was used, for several cases of mismatch between the domains of the two attached crystals. The analytical value is calculated based on (6), and marked by a *solid line*. The numerical results are marked by + for $\Delta L = 0$, by o for $\Delta L = 0.25L_c$, by x for $\Delta L = 0.5L_c$, and by $*$ for $\Delta L = L_c$

Note that unlike the former case of bonding two crystals one after the other, the power penalty when two crystals are put one on top of the other is always less than 100%.

In Figs. 4 and 5, the intensity distribution of the second-harmonic wave at the output facet of a 1-cm-long crystal pair is shown, for several different cases of domain mismatch under loose ($\xi = 0.01$) and tight ($\xi = 10$) focusing, respectively. When there is no mismatch, the output wave is a perfect Gaussian beam, but as the mismatch increases, areas of destructive interference can be observed, owing to mixing between fields generated in the two crystals with different phases. For loose focusing, the destructive interference is confined to the area near the interface between the two crystals, whereas for tight focusing the upper or lower lobes of the beams may be nearly completely destroyed. This can

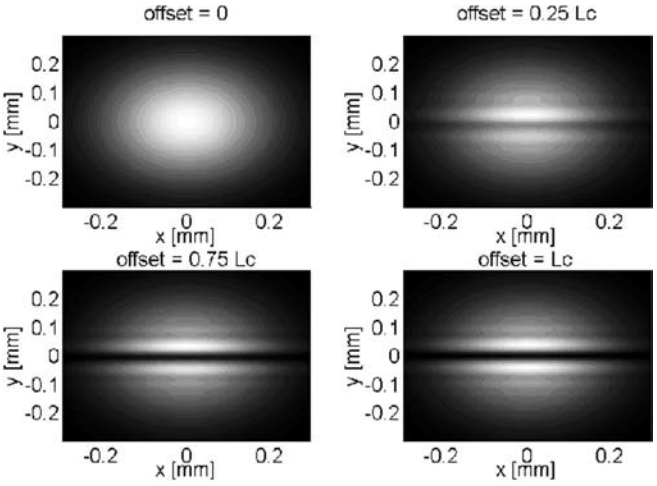

FIGURE 4 Intensity distribution of the second-harmonic field generated in 1-cm-long PPKTP crystal, for four different cases of domain mismatch, for loose focusing ($\xi = 0.01$)

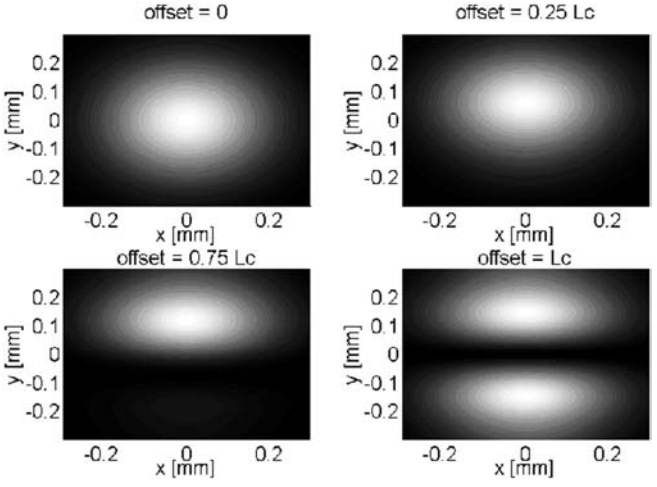

FIGURE 5 Intensity distribution of the second-harmonic field generated in 1-cm-long PPKTP crystal, for four different cases of domain mismatch, for tight focusing ($\xi = 10$)

be understood by comparing the relation between the beam width and its angular distribution. For a Gaussian beam with a waist ω_0, most of the energy is confined to a cone of light with a diffraction angle of $\lambda/\pi\omega_0 n$; hence after a crystal of length L this will generate a circular beam with a radius of $L\lambda/\pi\omega_0 n$. Part of the beam will then interfere with light generated in the other crystal. The radius of the diffraction circle becomes equal to the beam-waist radius for a focusing parameter of 0.5. For weak focusing, this radius is small compared to the beam radius; thus the destructive-interference effects are confined to a small area near the boundary between the two crystals. However, for tight focusing, the interference effects are much more pronounced, owing to the larger overlap between the light beams generated in the top and bottom crystals. This phenomenon is also in agreement with the results of Fig. 3, where for loose focusing the effect of domain mismatch on efficiency is much smaller than in the case of tight focusing.

In Fig. 5 one can observe that the lower lobe of the beam is nearly completely destroyed for a mismatch of $0.75L_c$. In this configuration, there is a phase difference of 0.75π between on-axis fields generated in the top and bottom crystals. However, the second-harmonic wave that is generated in one crystal and reaches the second crystal accumulates an additional phase φ owing to the longer path it travels. Hence, the phase difference in the bottom section will be $0.75\pi + \varphi$, and in the top section $0.75\pi - \varphi$. If φ is 0.25π, the optical field will be destroyed only in the bottom part. Note that, for a mismatch of $1.25L_c$, the mirror image is obtained, where the top lobe is nearly completely destroyed. In a similar fashion, a mismatch of $1.75L_c$ is the mirror image of the $0.25L_c$ mismatch, shown in that figure. It should be noted that this asymmetry between the intensity distributions of the top and bottom parts also takes place for loose focusing (e.g. in Fig. 4), but is more difficult to observe.

5 Experimental setup

The setup of Fig. 6 was used to evaluate the dependence of SHG power on the domain relative locations between two crystals. Two KTP crystals were z-cut and then periodically poled using an electric field poling process with a period of 24.7 μm for first order quasi phase matching the SHG at $\lambda \sim 1550$ nm. The crystals had the dimensions $3.5 \times 1 \times 14\,\text{mm}^3$, and they were polished at $\approx 44.7°$ at one of their edges. One crystal was attached to a static mount while the other crystal could be translated vertically using a micrometer. This crystal was pushed using a spring in the horizontal direction in order to maintain physical contact with the static crystal. This configuration enabled us to continuously change the relative phase of the domains of the two crystals. An index-matching liquid with $n = 1.657$ at 775 nm, 25 °C, $n = 1.643$ at 1550 nm, 25 °C was used to prevent total internal reflection in the interface between the two crystals. Better index matching can be achieved using higher refractive index liquids, but such liquids were avoided because of their toxicity. The fundamental beam was a TEM_{00} longitudinal mode from a single mode fiber of a tunable laser, which was set to a wavelength of 1548.15 μm. The polarization and wavelength were optimized to yield the highest SHG efficiency at room temperature.

The setup enabled us to evaluate the ability of increasing the crystal's length but not its thickness. Trying to evaluate the thickening of the crystal involves several experimental difficulties: on the one hand the beam should propagate parallel to the interface between the two crystals, overlapping this area during its propagation along the crystal. On the other hand, letting one of the crystals move in order to measure several domain mismatches requires a separation layer in the interface to provide smooth movement between the crystals. The interface between the crystals should be polished and, for preventing total internal reflection of the propagating field from the interface between the crystals, high index matching liquid should be used. Another difficulty is that the beam is directed to the interface between the crystals, which is nonideal for optical interactions, due to small cracks and inhomogeneities in the crystal's corners. Although such a setup had been built, we have not observed the expected modulation so far.

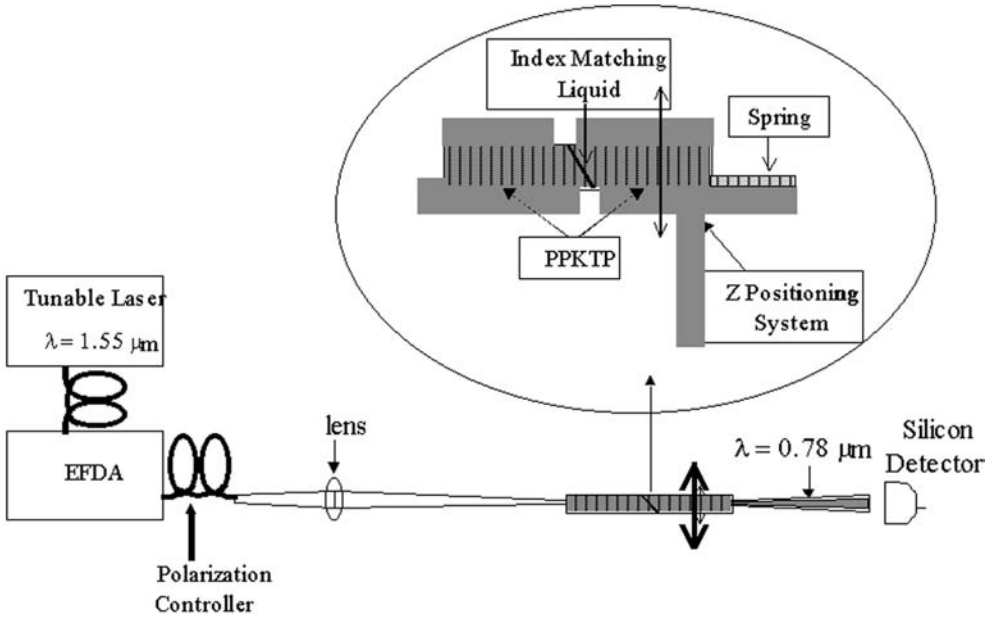

FIGURE 6 The experimental setup for measuring the effect of domain mismatch on second-harmonic power. *Inset* shows the area of contact between the two crystals

6 Experimental results

The experimental results obtained from the setup shown in Fig. 6 were in good agreement with the expected behavior. Figure 7 shows the measured second harmonic power modulation as a result of lifting the mobile crystal, compared to the analytical and numerical results expected from the domain mismatch caused by this movement. The period of the power modulation was measured to be 25.9 μm, with 95% modulation depth. The error between the expected modulation period, which equals the mask period and the measured modulation period, can be explained by a non-perpendicularity of $\sim 2.6°$ between the micrometer-movement direction and the beam-propagation direction (which is assumed to be perpendicular to the input and output facets of the crystal pair). From 22 mW at $\sim$ 1548.15 nm, with a beam waist of 64.5 μm, 523 nW of second-harmonic power was generated, yielding an efficiency of 0.052%/W cm with respect to the expected analytical efficiency of 0.248%/W cm. The low efficiency might be explained by non-optimal orientation and polarization of the fundamental beam, reflection losses at the interface between the two attached crystals and the index matching liquid layer between them, and non-optimal orientation of the two crystals. From (6) one can derive the effective non-linear coefficient, which in this experiment was found to be 3.91 pm/V, with respect to the theoretical value for an ideal periodically poled crystal of 8.52 pm/V (following [24], and taking Miller's delta into account [25]). The power decay between following periods is due to mechanical instability of the setup. An explanation for the non-optimal modulation depth can be a non-optimal position of the beam waist with respect to the two crystals.

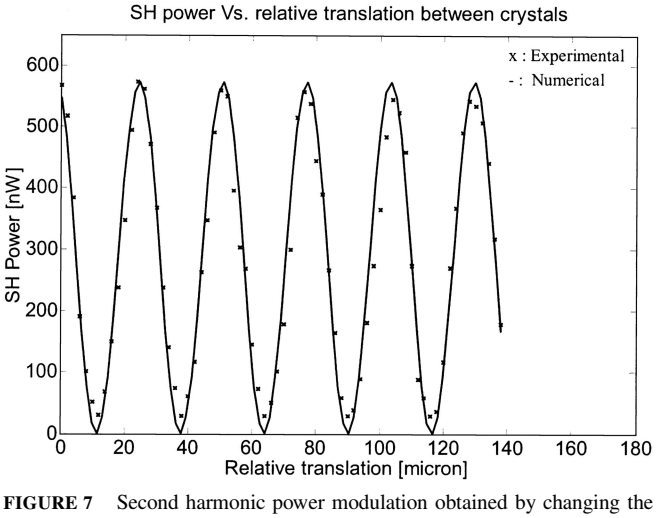

FIGURE 7 Second harmonic power modulation obtained by changing the relative mismatch between the two crystals. The experimental results x are compared to analytical results normalized to the maximal measured power and the measured periodicity (*solid line*)

From the experimental results the importance of the relative phase of the domains in the two crystals is clear, and the setup demonstrates a useful method for attaching two crystals for gaining the optimal phase match between the two separated crystals.

7 Discussion and summary

The severe sensitivity of non-linear frequency-conversion processes to the domain mismatch in diffusion bonded periodically poled crystals is discussed. The effect is demonstrated and the tolerances are defined numerically for two cases of diffusion bonded PPKTP crystals: two crystals attached one on top of the other as a technique for thickening the crystal, and crystals attached one after the other as a technique for enlarging the crystal. While the power modulation expected for the first configuration is somewhat less severe and found numerically to be limited to 34% of the optimal efficiency for the optimal focusing condition, for the second configuration the second-harmonic power may be completely destroyed. We have found that the second harmonic intensity

distribution in the configuration in which the crystals are one on top of the other is strongly dependent on the phase mismatch and focusing conditions. In some cases, an asymmetric intensity distribution is observed.

This sensitivity is experimentally demonstrated for the configuration of increasing the crystal length, where full destructive interference causes total extinction of the second-harmonic power.

The numerical simulation described above can be easily generalized for other frequency-mixing processes such as sum- and difference-frequency generation, and for arbitrary beam shapes. The simulation can be also generalized for three-dimensional periodically poled crystals, and the expected beam shape can be found.

The experimental setup described in Sect. 5 can be used for locating the optimal relative location between two or more diffusion bonded periodically poled crystals before the bonding stage takes place. Using this method three-dimensional non-linear periodically poled crystals can also be created using a multi-crystal configuration.

Based on the diffusion bonding method, a configuration that guarantees a predicted worse-case efficiency can be offered, for both increasing the length (Fig. 8a) and increasing the thickness (Fig. 8b) configurations. This configuration (shown in side view) is based on using two periodically poled crystals one of which will be poled in the 'conventional' way, while the other will be poled using a mask with separated sections, where each section will have a predetermined offset from its predecessor, as shown in the upper part of Fig. 9 (shown in top view). Using this method the amount of worse-case power degradation can be found and minimized, such that for a graded offset crystal with eight sections, the SHG efficiency for $0.1 \leq \xi \leq 4$ will be higher than 88% of standard QPM SHG for the configuration of increasing the crystal's length (see Fig. 9a). For $0.1 \leq \xi \leq 10$ the predicted efficiency will be better than 98% of standard QPM SHG for the configuration of increasing the crystal's thickness (see Fig. 9b). The arrows in Fig. 9 indicate the section of the optimal domain matching for the two configurations. The graded offset crystal should be wide enough to allow this configuration, and its minimum width is equal to the product of the number of sections times the thickness.

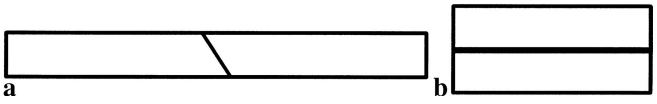

FIGURE 8 Minimal power degradation configurations for increasing the crystal length (**a**) and thickness (**b**) using shifted diffusion bonded crystals (*side view*)

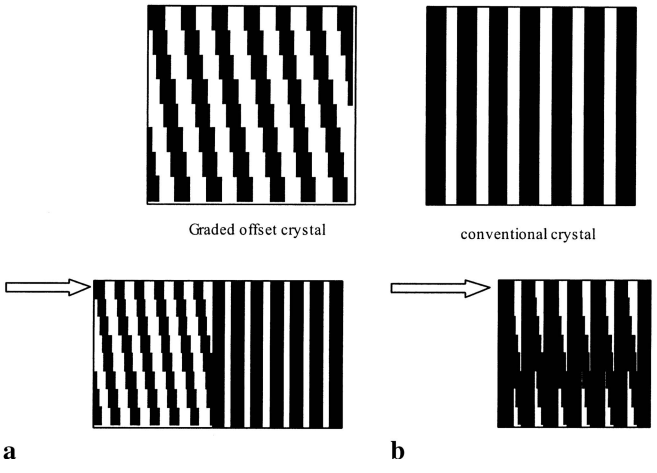

FIGURE 9 Demonstration of the functionality of the proposed configuration for limiting the degradation in SHG power using diffusion bonded crystals for both increasing the length (**a**) and thickness (**b**) of the crystal (*top view*). *Black and white areas* represent regions with opposite sign of the non-linear coefficient

ACKNOWLEDGEMENTS This work was partly supported by the Israeli Ministry of Science.

REFERENCES

1 G. Rosenman, A. Skaliar, A. Arie: Ferroelectr. Rev. **1**, 263 (1999)
2 J. Hellstrom, V. Pasiskevicius, F. Laurell, H. Karlsson: Opt. Lett. **25**, 174 (2000)
3 H. Karlsson, M. Olson, G. Arvidsson, F. Laurell, U. Bader, A. Borsutzky, R. Wallenstein, S. Wickstrom, S. Gustafsson: Opt. Lett. **24**, 330 (1999)
4 L.E. Myers, T.P. Grayson, W.R. Rosenberg, M.D. Nelson, V. Dominic, M.M. Fejer, R.L. Byer: In: OSA Tech. Dig. Conf. Lasers Electro-optics (1996) p. 9
5 L.M. Myers, R.C. Eckardt, M.M. Fejer, R.L. Byer, W.R. Bosenberg: SPIE **2700**, 216 (1997). Although this is the longest commercial bulk PPLN crystal, a PPLN length of up to 86 mm had been achieved (see for example G. Schreiber et al.: Appl. Phys. B **73**, 501 (2001))
6 G. Rosenman, A. Skliar: Ferroelectrics **221**(1–4), 129 (1999)
7 G. Imeshev, M. Proctor, M.M. Fejer: Opt. Lett. **23**, 165 (1998)
8 J.M. Yarborough, J. Falk, C.B. Hitz: Appl. Phys. Lett. **18**, 70 (1971)
9 G.C. Bhar, U. Chatterjee, P. Datta: Appl. Phys. B **51**, 317 (1990)
10 K. Eda, M. Sugimoto, Y. Tomita: Appl. Phys. Lett. **66**, 827 (1995)
11 Y. Tomita, M. Sugimoto, K. Eda: Appl. Phys. Lett. **66**, 1484 (1995)
12 M. Missey, V. Dominic, L.E. Myers, C. Littell, R.C. Eckardt: OSA TOPS **10** (Adv. Solid State Lasers), 247 (1997)
13 M. Missey, V. Dominic, L.E. Myers, R.C. Eckardt: Opt. Lett. **23**, 664 (1998)
14 J.J. Zondy, M. Abed, S. Khodja: SPIE **2700**, 66 (1996)
15 G. Rosenman, A. Skliar, D. Eger, M. Oron, M. Katz: Appl. Phys. Lett. **73**, 3650 (1998)
16 A. Sennaroglu, A. Askar, F.M. Atay: J. Opt. Soc. Am. B **14**, 356 (1997)
17 A. Douillet, J.J. Zondy, A. Yelisseyev, S. Lobanov, L. Isaenko: J. Opt. Soc. Am. B **16**, 1481 (1999)
18 D.A. Kleinmann, R.C. Miller: Phys. Rev. **148**, 302 (1966)
19 G.D. Boyd, D.A. Kleinmann: Appl. Phys. **39**, 3596 (1968)
20 V. Berger: Phys. Rev. Lett. **81**, 4136 (1998)
21 B.E.A. Saleh, M.C. Teich: *Fundamental of Photonics* (Wiley, New York 1991)
22 D. Marcuse: *Theory of Dielectric Optical Waveguides* (Academic, San Diego 1991)
23 M.D. Feit, J.A. Fleck: Appl. Opt. **17**, 3990 (1978)
24 A. Arie, G. Rosenman, V. Mahal, A. Skliar, M. Oron, M. Katz, D. Eger: Opt. Commun. **142**, 265 (1997)
25 R.C. Miller: Appl. Phys. Lett. **5**, 17 (1964)